

Momentum distributions of sequential ionization generated by an intense laser pulse

N. I. Shvetsov-Shilovski,^{1,2,3} A. M. Sayler,^{1,2} T. Rathje,^{1,2} and G. G. Paulus^{1,2,4}

¹*Institute for Optics and Quantum Electronics, Friedrich-Schiller-University, Max-Wien-Platz 1, D-07743 Jena, Germany*

²*Helmholtz Institut Jena, Max-Wien-Platz 1, D-07743 Jena, Germany*

³*National Research Nuclear University MEPI, Kashirskoe shosse 31, Moscow, Russia*

⁴*Department of Physics, Texas A&M University, College Station, Texas 77843, USA*

(Received 7 December 2010; published 3 March 2011)

The relative yield and momentum distributions of all multiply charged atomic ions generated by a short (30 fs) intense (10^{14} – 5×10^{18} W/cm²) laser pulse are investigated using a Monte Carlo simulation. We predict a substantial shift in the maximum (centroid) of the ion-momentum distribution along the laser polarization as a function of the absolute phase. This effect should be experimentally detectable with currently available laser systems even for relatively long pulses, such as 25–30 fs. In addition to the numerical results, we present semianalytical scaling for the position of the maximum.

DOI: [10.1103/PhysRevA.83.033401](https://doi.org/10.1103/PhysRevA.83.033401)

PACS number(s): 32.80.Fb, 32.80.Wr

I. INTRODUCTION

The interaction of strong laser pulses with atoms and molecules results in a large number of different phenomena, among which are the formation of the high-energy plateau in the above-threshold ionization (ATI) spectrum, the generation of high harmonics of the incident field (HHG), and the excessive yield of doubly and multiply charged ions (see reviews [1–5]). The respective phenomena have been studied extensively in the last two decades, both theoretically and experimentally. These investigations were initially concerned with the total ion yield and the dependence of this yield on the intensity. Most of them dealt with double ionization and two different mechanisms underlying the production of doubly (or multiply) charged ions were revealed: nonsequential and sequential double (multiple) ionization.

The term nonsequential double (or multiple) ionization refers to the situation in which two (or more) electrons are ionized in one coherent process and the rate is not the product of single ionization rates. Hence, electron-electron correlation is a necessary condition of the nonsequential double ionization process. Nonsequential ionization is observed at relatively low laser intensities. It was first proposed in Refs. [6,7] that a nonsequential channel contributes to double ionization. The actual mechanism of this correlation was investigated and debated for many years. Finally, a consensus (i.e., that the dominating contribution to nonsequential double ionization is due to recollision [8,9]) has been achieved. The recollision process is also responsible for the ATI plateau and the HHG [9,10]. However, the details strongly depend on the atomic species (see [11] for reviews). When intensities increase such that the magnetic components of the electromagnetic field become significant, nonsequential ionization is suppressed. As a consequence, sequential ionization is predicted to dominate. This process is of considerable importance in view of the rapid increase in the intensity of currently available lasers. Another situation where sequential ionization may dominate is ionization by a circularly polarized field. For elliptical polarization, electrons have to start with nonzero initial velocity perpendicular to the main axis of the polarization ellipse in order to return to the position of the ion. However, this initial velocity decreases the tunneling rate. As a consequence,

the levels of the ATI plateau as well as the nonsequential double ionization (NSDI) rate decrease quickly with increasing ellipticity. Thus, in the case of a circular polarization, the nonsequential channel is essentially suppressed.

Due to the capabilities of modern experiments (especially since the advent of cold-target recoil-ion-momentum spectroscopy), both the total yield and the ion-momentum distributions can be measured [12–18]. It was found that, at high laser intensities, momentum distributions of multiply charged ions along the polarization direction have a Gaussian-type shape with the maximum at zero momentum [14,15,19].

In our laboratory, an experiment aimed at investigating the ionization dynamics with ion beams of well-defined charge state is under construction. In order to establish what to expect based on the current understanding of multiple ionization at high intensities, we investigate sequential ionization theoretically. Clearly, we do not expect perfect agreement between the forthcoming experimental data and the predictions of any model based on the sequential mechanism, especially at relatively low intensities. Nevertheless, such a model will provide a necessary benchmark for the data analysis and, no doubt, will help to understand the real pathways of the multiple ionization process.

At first glance, sequential ionization may appear trivial as compared to the nonsequential process. Consequently, most studies have focused on the latter ionization mechanism and there is, in fact, a lack of theoretical studies of sequential multiple ionization. Although the sequential ion yield was calculated by many groups (see [20–27] and references therein), emphasis has been put on the derivation of empirical formulas, which can describe the well-known “knee” in the ion yield, caused by the presence of the nonsequential channel. The aforementioned lack of relevant theory becomes particularly evident in the case of momentum distributions. Momentum distribution of multiply charged ions up to $Z = 8$ produced by a strong laser pulse with duration of 200 fs and maximum intensity of $5–7 \times 10^{15}$ W/cm² were recently measured and calculated in Refs. [28,29]. To the best of our knowledge, Refs. [28,29] are the only theoretical studies of the momentum distributions of the highly charged ions. Ionization dynamics was simulated using the classical trajectory Monte Carlo method including tunneling (CTMC-T method, see [30,31]). It

has been found experimentally that the width of the momentum distribution along the polarization direction is almost a linear function of the ionization potential. This linear dependence was explained on the basis of the strong-field approximation and electron kinematics in the laser field.

Nevertheless, the momentum distributions of highly charged ions have not been analyzed so far. This requires analyzing the subcycle ionization dynamics, whereas previous work has concentrated on the pulse envelope. Moreover, sequential multiple ionization by *short* laser pulses has not been investigated including the corresponding carrier-envelope phase (CEP) effects (see review [32] and references therein). In this paper, we further explore the sequential ionization in order to (i) calculate momentum distributions of ion with $Z \geq 8$; (ii) consider the ion production by a short laser pulse, when the CEP effects may be relevant; and (iii) find out the scaling of momentum distributions with laser-atom parameters.

II. EXPERIMENTAL SETUP

In this section, we briefly describe the experimental setup under construction in our laboratory and that we have in mind in our theoretical study. An ion beam is produced in an EBIT (electron beam ion trap) that is kept at a potential of approximately 5 kV, and which can produce xenon ions with charges ranging from Xe^{1+} to around Xe^{20+} .

Selecting the desired initial charge state with a Wienfilter (WF) [33] allows for determining the effects of the initial charge state on the subsequent laser-induced ionization. Einzel lenses (EL1, EL2), deflector plates (DF1, DF2, DF3), and adjustable pinholes (AP1, AP2) shown in Fig. 1 are used to produce a well-collimated ion beam at the laser interaction point (IA).

The focused laser beam is linearly polarized in the x direction, which is orthogonal to the ion beam propagation in the y direction, and hits the ion beam in the interaction region (IA). The momentum distribution of the ions in the y direction arises from the acceleration of the charged nuclei in the laser field.

After the laser interaction, the charge separator (CS) deflects the ions in the z direction using an electrostatic field. The nonionized portion of the ion beam is collected in a Faraday cup (FC), while the different ionization states are separated in space. The charge state and momentum distributions are then

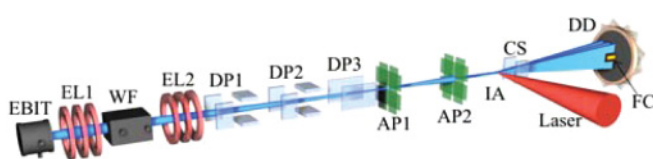


FIG. 1. (Color online) Experimental setup of the ion beam apparatus, which includes an electron beam ion trap (EBIT), two Einzel lenses (EL1, EL2), a Wienfilter (WF), three deflector plates (DF1, DF2, DF3), two adjustable pinholes (AP1, AP2), an interaction region (IA), a charge separator (CS), a Faraday cup (FC), and a delay-line detector (DD). The laser beam is focused vertically linear polarized into the ion beam.

detected using a time- and position-sensitive microchannel plate (MCP) delay-line detector (DD).

III. MODEL

In this section, we will sketch our numerical technique with special emphasis on the details that are essential for the following. Let us consider a short laser pulse with the duration $\tau_L = (2\pi/\omega)n_p$ and a sine-square envelope, linearly polarized along the x axis:

$$F(t) = F_0 \sin^2(\pi t/\tau_L) \cos(\omega t + \varphi), \quad (1)$$

where n_p is the number of cycles within the pulse and ω is the carrier frequency.

In a strong field of laser radiation, an ionized electron can obtain relativistic energy in the final continuum state that is on the order of its rest energy. Taking into account that the oscillation energy of a free electron is $F^2/4\omega^2$, one can easily find that relativistic effects occur for radiation of the Ti:Sa laser at the intensity greater than $5 \times 10^{18} \text{ W/cm}^2$ (see Ref. [2]). In our study, we will not consider intensities exceeding this value. More importantly, we consider the ion momentum, which will remain nonrelativistic even for much higher intensities.

A. Rate equations

Consider neutral atoms with a charge $Z = 0$ and initial momentum \mathbf{P}_0 exposed to a short intense laser pulse. Let N be the maximal ion charge that can be achieved for a given laser intensity and $R_Z(t)$ denote the probability for an ion to have charge Z at a given time instant t . Let $W_Z(t) \equiv W_Z(F(t), I_Z)$ be the ionization rate for an ion with the charge Z and ionization potential I_Z . Assuming that ions are created in a sequential process, we obtain the following system of rate equations:

$$\begin{aligned} \frac{dR_0}{dt} &= -W_0 R_0, \\ \frac{dR_1}{dt} &= W_0 R_0 - W_1 R_1, \\ \frac{dR_2}{dt} &= W_1 R_{Z+1} - W_2 R_2, \\ &\dots, \\ \frac{dR_N}{dt} &= W_N R_{N-1}. \end{aligned} \quad (2)$$

The initial conditions read as $R_0(0) = 1$ and $R_Z(0) = 0$ for $Z = 1, 2, \dots, N$. Adding all the equations of the system (2), we get the conserved quantity

$$R_0(t) + R_1(t) + \dots + R_N(t) = 1. \quad (3)$$

Equation (3) is a constraint under which the system of rate equations (2) needs to be solved. A glance at the result (see Fig. 2) that will be obtained reveals that only two to three terms that sum in Eq. (3) differ from zero at any given time instant.

The system of equations (2) has already been solved by many authors (see [20–22, 24–26] and references therein) for different atomic species and within a wide range of laser parameters. Particularly worth noting is the semianalytical

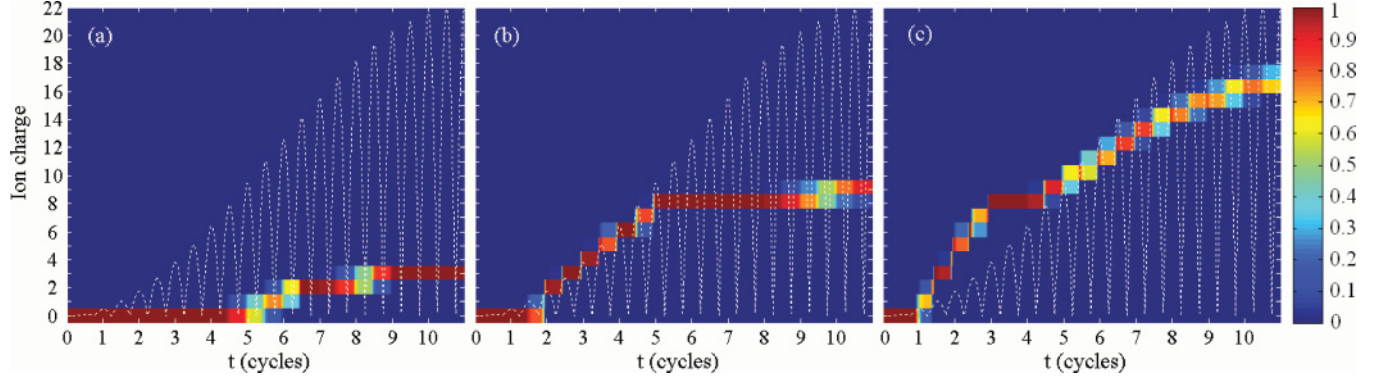


FIG. 2. (Color online) Results of the numerical solution of the rate equations (2) for Xe ions. Three panels (a), (b), and (c) correspond to peak intensities of 0.8, 60, and 500×10^{15} W/cm², respectively. The color scale depicts the time-dependent ionization state distribution. In all cases, the pulse duration is 30 fs at FWHM and the white line is the instantaneous intensity.

approach developed in [21], based on the following formal solution of Eqs. (2):

$$\begin{aligned} R_0(t) &= \exp \left\{ - \int_{-\infty}^t W_0(t') dt' \right\}, \\ R_1(t) &= \exp \left\{ - \int_{-\infty}^t W_1(t') dt' \right\} \int_{-\infty}^t \exp \left\{ \int_{-\infty}^s W_1(t') dt' \right\} \\ &\quad \times R_0(s) W_0(s) ds, \\ R_2(t) &= \exp \left\{ - \int_{-\infty}^t W_2(t') dt' \right\} \int_{-\infty}^t \exp \left\{ \int_{-\infty}^s W_2(t') dt' \right\} \\ &\quad \times R_1(s) W_1(s) ds, \\ &\quad \dots, \\ R_N(t) &= \int_{-\infty}^t W_{N-1}(s) R_{N-1}(s) ds. \end{aligned} \quad (4)$$

After some approximations, this formal solution (4) can be simplified, and, by doing so, analytic estimates can be derived [21].

The aforementioned solutions of rate equations were obtained for Gaussian [22,24], Lorentzian [25,26], and hyperbolic-secant [21] pulse envelopes. To the best of our knowledge, the oscillations of the laser field have not been taken into account for solving Eqs. (2). However, knowing the cycle-resolved ionization dynamics is necessary to compute the momentum distribution of a given ion. Due to these reasons, we start our theoretical study from the solution of the rate equations (2).

B. Ionization rates

In order to solve system (2), one needs to know the ionization probabilities $W_Z(t)$. For such probabilities, we can use the ionization probability by a static field [34] or by Perelomov-Popov-Terent'ev [35] or Ammosov-Delone-Krainov (ADK) [36] formulas. Then, the tunneling rate for a level with ionization potential I_p reads as

$$\begin{aligned} W_{l,m} &= (2I_p)(2l+1) \frac{(l+m)!}{2^m m! (l-m)!} C_{kl}^2 2^{2n^*-m} \\ &\quad \times \left(\frac{F}{F_a} \right)^{m+1-2n^*} \exp \left(-\frac{2F_a}{3F} \right). \end{aligned} \quad (5)$$

Here $F_a = (2I_p)^{3/2}$ is the atomic field, $n^* = Z/\sqrt{2I_p}$ is the effective quantum number, C_{kl}^2 is the asymptotic coefficient of the atomic wave function (see [37] for details), and l and m are the angular and magnetic quantum numbers, respectively. Atomic units ($e = m = \hbar = 1$) are used throughout the paper. We omit the Keldysh parameter $\gamma = \omega\sqrt{2I_p}/F$ in the exponent of Eq. (5), and, of course, the pre-exponential factor $\sqrt{3\pi/F}$, because the latter arises from the averaging over the laser period.

Simple estimates show, however, that neutral Xe atoms, as well as Xe⁺ and Xe²⁺ ions, are ionized in the barrier-suppression regime even at an intensity of 10^{14} W/cm². This means that, strictly speaking, we need to use ionization rates suitable for barrier suppression ionization in Eqs. (2).

Ionization by a field $F \geq F_{BSI}$, where F_{BSI} is the field strength, when the perturbed energy of the initial state exceeds the maximum of an effective potential barrier was analyzed by many authors (see Refs. [38–42]). However, it is well known that, presently, no universal nonempirical formulas for the ionization probability in the barrier-suppression regime are in agreement with solutions of the time-dependent Schrödinger equation (TDSE) (see Ref. [40]).

An exception, however, is the result by V. S. Popov *et al.* [37,41] based on the investigation of the Stark effect [43–46], i.e., the probability was calculated as a width of the corresponding Stark level. However, these results are appropriate for atomic hydrogen only and their generalization to other atomic species is not obvious.

A simple empirical formula (both for the tunneling and the barrier-suppression regime) with only one free parameter has recently been proposed by X. M. Tong and C. D. Lin [42]. This parameter, however, must be computed by comparing with the TDSE solution for any given initial state.

For low-frequency laser fields, the barrier-suppression ionization rate was calculated by V. P. Krainov [38,39] on the basis of the strong-field approximation. This rate reduces to the usual ADK rate [36] in the tunneling limit when the laser field is relatively weak: $F \ll F_{BSI}$. Note that the Stark shift of the initial bound state was not taken into account in the derivation of the formulas in Refs. [38,39]. As a consequence, this formula can give results only in qualitative agreement with the solution of TDSE, considerably overestimating the

ionization probability in the above barrier region [40]. In addition, the result of Refs. [38,39] is averaged over one laser cycle and valid only for s and p states (in the latter, the averaging over $m = -1, 0, 1$ is performed).

Let us generalize the rate [38,39] for the case of an arbitrary orbital momentum of the initial state and avoid averaging over the laser period. By doing so, we get the following expression:

$$W_{l,m} = \sqrt{\pi}(2I_p)(2l+1) \frac{(l+m)!}{2^m m! (l-m)!} C_{kl}^2 2^{2n^* + \frac{14}{3} - m} \\ \times \left(\frac{F}{F_a} \right)^{m + \frac{1}{6} - 2n^*} \int_0^\infty \text{Ai}^2(k^2 + x^2) x^2 dx, \quad (6)$$

where $k = 2I_p / (2F)^{2/3}$ and Ai denotes the Airy function.

In the following, we will use mainly the probability Eq. (6). However, as we will see below in Sec. IV A, there is no essential difference as to which formula [Eq. (5) or (6)] is used in the calculations. Moreover, we will consider these expressions as the ionization probabilities by a static field. In other words, for solving the rate equations, we will substitute not the envelope, as was done before in Refs. [21,25,26], but the instantaneous laser field in the formulas for $W_{l,m}$. To be more specific, we will use the modulus of Eq. (1), i.e., $F_0 \sin^2(\pi t/\tau_L) |\cos(\omega t + \varphi)|$, instead of F in the ionization rates [Eqs. (5) and (6)].

C. Derivation of the momentum distributions

The calculation of the ion-momentum distribution is not quite as simple as it may appear at first glance. The fact is that the depletion of the ions with the preceding charge $(Z-1)$ should be taken into account when calculating the distributions of ions with charge Z .

Our solution of the problem is based on a Monte Carlo algorithm, which has some important peculiarities that are briefly described here. The simulations are based on the calculation of the trajectory of a particle (the ion) in the laser field taking into account the possibility for this particle to be ionized by the field once, or many times, during the pulse. For the simulation, the temporal axis is discretized, i.e., subdivided into small intervals. The trajectory of the ion must be analyzed in each of the intervals. We start from the neutral atom $Z=0$ with zero initial velocity along the laser polarization $P_x=0$. Obviously, the laser field does not act on the neutral particle, but it will act on the particle, as soon as it is ionized.

Assume that $P_x(t_0)$ and Z are the momentum and the charge of the particle at a certain instant t_0 , respectively. Let us then take a look at the interval $(t_0, t_0 + \Delta t)$. The ion momentum at the end of this interval can be calculated according to Newton's equation

$$P_x(t_0 + \Delta t) = P_x(t_0) + Z \int_{t_0}^{t_0 + \Delta t} F(t') dt'. \quad (7)$$

On the other hand, the probability for an ion of charge Z to be ionized during the interval Δt can be calculated as $W_Z(t_i) \Delta t$; or, more exactly, as $\int_{t_0}^{t_0 + \Delta t} W_Z(t) dt$. This probability is evaluated and compared with a random number $0 \leq x \leq 1$. If the probability is greater than the random number, then the

next ionization occurs and the charge of Z is increased by one. This means that, for the next time interval $(t_0 + \Delta t, t_0 + 2\Delta t)$, we consider the motion of an ion with charge $(Z+1)$. In the opposite case, when the ionization probability is smaller than our random number x , the particle is not ionized during the interval $(t_0, t_0 + \Delta t)$. In both cases, the particle starts its motion on the next time interval with the momentum $P_x(t_0 + \Delta t)$ [see Eq. (7)]. Thus, at the end of the pulse, we obtain an ion of a certain charge Z_F and with a certain momentum $P_{F,x}$. By using an ensemble of such trajectories, one can get the necessary statistics to calculate momentum distributions.

IV. RESULTS AND DISCUSSION

A. Solution of the rate equations

For solving system (2), one can use the standard numerical method such as the Runge-Kutta method with adaptive step-size control (see, e.g., [47]). However, the rate equations are stiff [21] because the tunneling rates $W_{k-1}(t)$ and $W_k(t)$ entering into the rate equation for the probability $R_Z(t)$ usually differ by more than one order of magnitude. Thus, it is reasonable to use numerical methods specially adapted to the solution of stiff differential equations, e.g., the Gear method [48].

Another possible approach is based on the formal solution (4). In this case, one has to evaluate a great number of definite and improper integrals. Although the integrands are positive, they oscillate very rapidly and it is important to prevent precision loss due to truncation errors.

We used both methods in order to check the consistency. The results obtained by both alternatives are in agreement. The characteristic probability for an ion to have a specific charge as a function of time is shown in Figs. 2(a)-2(c) at three different intensities. For visual convenience, the instantaneous laser intensity is also shown on the figure. These results provide detailed information about the ionization dynamics of an ionic target. Our numerical analysis shows that barrier-suppression ionization plays a minor role in the production of highly charged ions, even for short laser pulses: Ions with $Z > 2$ are ionized before the intensity reaches the corresponding barrier-suppression value. This result is in agreement with the conclusion of Ref. [28] for long pulses.

In addition to, and aside from, other aspects, our calculations deliver the time intervals when different highly charged ions exist within the pulse (see Fig. 2). These intervals can easily be transformed into respective intensity regions. It should be mentioned that the boundaries of these intensity regions, i.e., threshold and saturation intensities, are in good quantitative agreement with the results of [21].

Another interesting question is which ion would dominate at the given intensity after the end of the laser pulse or, vice versa, which intensity is necessary to maximize the yield of a given ion. The latter dependence has been calculated and is shown in Fig. 3. The entire dependence can be fitted by a quadratic function. The two big groups of points on this

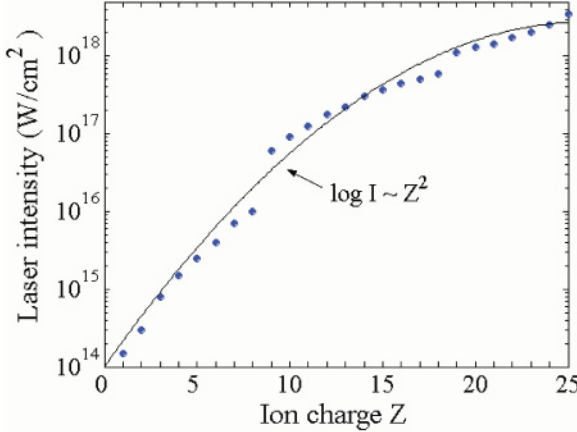


FIG. 3. (Color online) The laser intensity, which maximizes the ion yield of a specific charge state, is shown as a function of the ion charge. The thin black line corresponds to the quadratic fitting: $\log_{10} I \propto Z^2$.

figure correspond to the atomic shells $5p^65s^2$ and $4d^{10}4p^64s^2$, subsequently ionized in our calculations.

B. Momentum distributions

The results of our simulation for the ion-momentum distributions are presented on Figs. 4, 5, and 6. It is seen from these figures that the ion-momentum distribution has a Gaussian shape. Any Gaussian-type curve can be characterized by two parameters: its width and the position of the maximum.

The dependence of the width of the ion-momentum distribution on the ionization potential I_p shown in Fig. 4 can easily be obtained as follows: For any given ion, there is an intensity that maximizes the yield of this ion (see Fig. 3). Thus, by performing the Monte Carlo simulations at this intensity, one can calculate the corresponding momentum distribution and obtain its width. It is reasonable that the width of the ion-momentum distribution increases with increasing laser intensity. At intensities of $5\text{--}7 \times 10^{16}$ W/cm², the widths of the momentum distribution of the product ions exhibit a linear

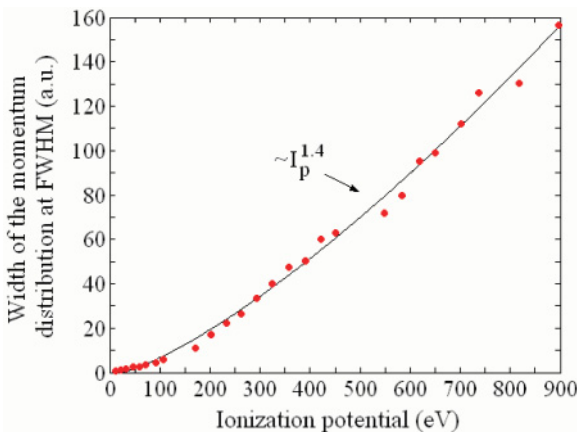


FIG. 4. (Color online) Width (FWHM) of the ion-momentum distribution as a function of ionization potential I_p . Numerical results are fitted to a power law $\propto I_p^{1.4}$ depicted by the thin black line.

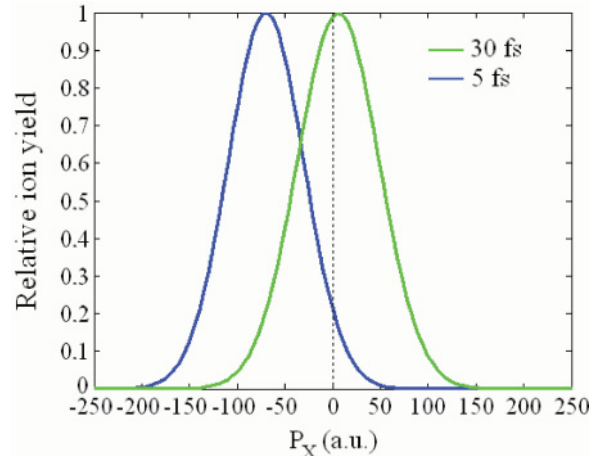


FIG. 5. (Color online) Ion-momentum distribution of Xe^{21+} at the intensity of 1.5×10^{18} W/cm² for two different pulse durations at FWHM. The shift of the maximum is clearly seen from the figure.

dependence on the ionization potential of the respective ions [28,29]. Such a linear dependence was analyzed theoretically using the strong-field approximation and a reasonable scaling was proposed [29]. However, our calculations show that, within a wider range of intensities ($10^{14}\text{--}10^{18}$ W/cm²), the width of ionic momentum distribution is proportional to $I_p^{1.4}$ (see Fig. 4).

Apart from the investigation of the widths, we predict a new effect: the shift of the maxima from zero momentum (see Fig. 5). This effect originates from the finite pulse duration and vanishes for a monochromatic field. It also vanishes when averaging over the carrier-envelope phase φ . Hence, this shift must be considered as a carrier-envelope phase effect. It would be very desirable to have a scaling for the shift. However, such a scaling is quite an intricate problem.

It is evident that ionization happens near field maxima, i.e., near minima of the vector potential. It would also appear reasonable that each ionization act occurs near its own maxima of the laser field. However, such a seemingly natural assumption is not true [see Fig. 2(c)]. For example, at the parameters of Fig. 2(c), we have one ionization event during the first half of the laser period, two events during the second half of period, etc. Thus, in order to estimate the position of the maxima at given laser-atom parameters, one has to solve the rate equations (2) first, i.e., one has to determine the subcycle ionization dynamics.

Once the ionization dynamics is known, one can easily derive the scaling of the shift of maximum. Indeed, according to momentum conservation

$$\mathbf{P} = - \sum_i \mathbf{p}_{e_i}, \quad (8)$$

where \mathbf{p}_e are the momenta of all ionized electrons after the end of the laser pulse.

Consider an electron ionized at instant of time t_0 . Then, the asymptotic momentum of the electron at $t \rightarrow \infty$ reads as

$$p_{e,x} = - \int_{t_0}^{\tau_L} F(t) dt. \quad (9)$$

Assuming that ionization happens exactly at field maxima $\omega t = \pi k$, one has, from Eq. (1),

$$p_{e,x} = \frac{F_0}{2\omega n_p} (-1)^{(k+1)} \sin\left(\frac{\pi k}{n_p}\right) \left(1 + \frac{1}{n_p^2}\right). \quad (10)$$

For simplicity, we assume that $\varphi = 0$ when calculating the last equation. In order to estimate the position of the maximum, one has to sum Eq. (10) over all the relevant values of k , which should be extracted from the solution of Eqs. (2). Note that the same value of k may appear in the sum of Eq. (10) several times if there are several ionization events on the corresponding half-cycle. For example, at the intensity of $5.0 \times 10^{17} \text{ W/cm}^2$ and for pulse duration of 30 fs (FWHM), the index k runs over the values (2,3,3,4,4,5,6,6,9,11,12,13,14,15,17,19) [see Fig. 2(c)]. In this case, we have, from Eqs. (8) and (10), $P_x \approx 2.3 \text{ a.u.}$, whereas the calculated momentum distribution of Xe^{16+} has its maximum at $P_x \approx 5.0 \text{ a.u.}$ It should be noted, however, that the estimate Eq. (10) is appropriate only if each ionization act can be assigned to a certain half-cycle. If this is not the case, i.e., the new charge state appears during several half of periods, this scaling gives wrong results.

The intensity and phase dependence of the centroid is shown in Fig. 6 for short and relatively long laser pulses. Here

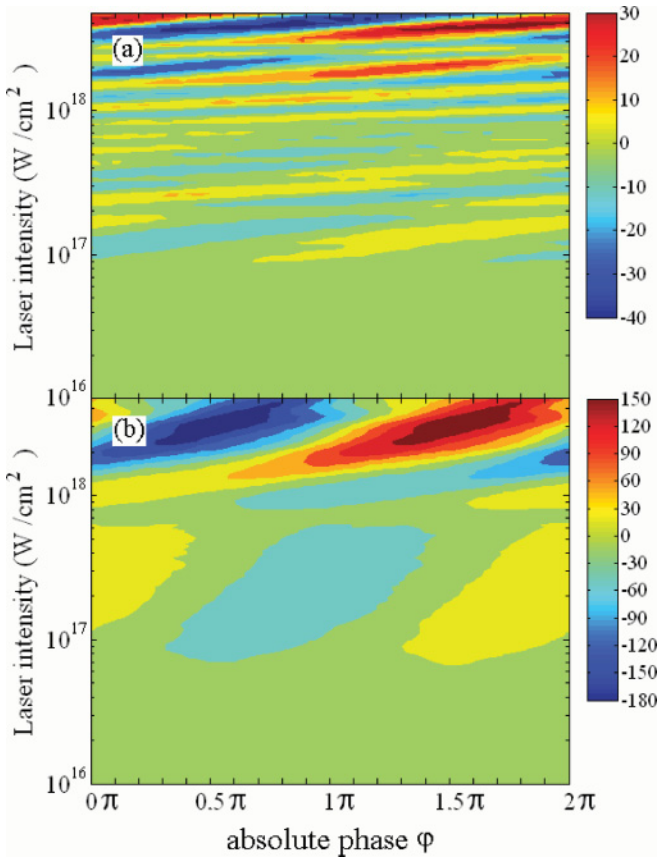


FIG. 6. (Color online) The shift of the centroid in atomic units as a function of the phase φ and intensity. At any given intensity only the distribution of the ion with the highest yield is considered. The two panels (a) and (b) correspond to the pulse duration of 30 and 6.7 fs at FWHM, respectively.

we briefly discuss both the intensity and phase dependence. It is evident from Eq. (10) that the shift of the maxima is proportional to the field strength and inversely proportional to the duration of the pulse. Because of this, the displacement of the maxima from $P_x = 0$ can be observed in long pulses [up to 30 fs at FWHM; see Fig. 6(a)] provided the intensity is high enough.

It should be mentioned that we were only discussing the momentum distribution of the charge state, which has the highest yield at the given peak intensity. The momentum distribution of other charge states, which arises after the end of the laser pulse, is also shifted. In principle, one can calculate the corresponding shifts as well. However, this calculation does not provide any additional information about the effect under consideration: As one would expect, the distributions of the lower charge states are less shifted than the distributions of the higher ones.

The strong dependence on the CEP originates from the different ionization pathways [different sets of k in Eq. (10)], which are realized at different values of the phase due to the different temporal evolution of the field. The phase dependence of the shift survives even for relatively long pulses [see Fig. 6(a)]. This may appear surprising. In fact, phase effects with respectively long pulses have been observed before in HHG under situations where contributions of different recolliding electron trajectories interfered [49]. Here the situation is completely different: The asymmetry is dominated by the ionization event occurring in the optical cycle next to the pulse maximum. Evidently, the phase effects for long pulses are hard to observe if focal averaging plays a significant role. Ion beam experiments have a distinct advantage in this respect.

V. CONCLUSIONS

In conclusion, we have investigated the total yields and the momentum distributions of highly charged ions produced by strong laser pulses at different intensities and pulse durations. We present numerical results as well as semianalytic estimates and scaling relations. A surprising result of our study is that the maximum of the longitudinal ion-momentum distribution shifts from zero momentum, even for pulses much longer than a few cycles provided the laser intensity is high enough. The magnitude of this shift is proportional to the field and inversely proportional to the pulse duration. This effect should be experimentally detectable for pulses of 25–30 fs duration at FWHM. In addition, we have demonstrated that, even for short pulses, barrier-suppression ionization plays a minor role in the production of multiply charged ions due to the temporal variation of the laser field. Consequently, tunneling is the most important mechanism of the multiple ionization.

ACKNOWLEDGMENTS

We are grateful to S. P. Goreslavski and W. Becker for fruitful discussions. The research was funded by Deutsche Forschungsgemeinschaft (DFG programmes SFB/TR18). This work was also partially supported by the Russian Foundation of Basic Research, Project No. 09-02-00773-a, and by the Federal Goal Program, Project No. P1546.

- [1] M. V. Fedorov, *Atomic and Free Electrons in a Strong Laser Field* (World Scientific, Singapore, 1997).
- [2] N. B. Delone and V. P. Krainov, *Multiphoton Processes in Atoms* (Springer, Berlin, 2000), Chap. 9.
- [3] W. Becker *et al.*, *Adv. At. Mol. Opt. Phys.* **48**, 35 (2002).
- [4] D. B. Milošević and F. Ehlotzky, *Adv. At. Mol. Opt. Phys.* **49**, 373 (2003).
- [5] A. Becker and F. H. M. Faisal, *J. Phys. B: At. Mol. Opt. Phys.* **38**, R1 (2005).
- [6] V. V. Suran and I. P. Zapesochny, Pis'ma Zh. Tech. Fiz. **1**, 420 (1975) [Sov. Tech. Phys. Lett. **1**, 420 (1975)].
- [7] A. l'Huillier, L. A. Lompré, G. Mainfray, and C. Manus, *Phys. Rev. A* **27**, 2503 (1983).
- [8] M. Yu. Kuchiev, Pis'ma Zh. Eksp. Teor. Fiz. **45**, 319 (1987) [Sov. Phys. JETP Lett. **45**, 404 (1987)].
- [9] P. B. Corkum, *Phys. Rev. Lett.* **71**, 1994 (1993).
- [10] J. L. Krause, K. J. Schafer, and K. C. Kulander, *Phys. Rev. Lett.* **68**, 3535 (1992).
- [11] R. Dörner *et al.*, *Adv. At. Mol. Opt. Phys.* **48**, 1 (2002); A. Becker, R. Dörner, and R. Moshammer, *J. Phys. B: At. Mol. Opt. Phys.* **38**, S753 (2005).
- [12] T. Weber *et al.*, *Phys. Rev. Lett.* **84**, 443 (2000).
- [13] R. Moshammer *et al.*, *Phys. Rev. Lett.* **84**, 447 (2000).
- [14] T. Weber *et al.*, *Nature (London)* **405**, 658 (2000).
- [15] T. Weber *et al.*, *J. Phys. B: At. Mol. Opt. Phys.* **33**, L127 (2000).
- [16] B. Feuerstein, R. Moshammer, and J. Ullrich, *J. Phys. B: At. Mol. Opt. Phys.* **33**, L823 (2000).
- [17] R. Moshammer *et al.*, *Phys. Rev. Lett.* **91**, 113002 (2003).
- [18] A. Rudenko *et al.*, *J. Phys. B: At. Mol. Opt. Phys.* **37**, L407 (2004).
- [19] A. Rudenko, K. Zrost, B. Feuerstein, V. L. B. de Jesus, C. D. Schröter, R. Moshammer, and J. Ullrich, *Phys. Rev. Lett.* **93**, 253001 (2004).
- [20] P. Lambropoulos and X. Tang, *J. Opt. Soc. Am.* **4**, 821 (1987).
- [21] Briton Chang, Paul R. Bolton, and David N. Fittinghoff, *Phys. Rev. A* **47**, 4193 (1993).
- [22] S. Augst, A. Talebpour, S. L. Chin, Y. Beaudoin, and M. Chaker, *Phys. Rev. A* **52**, R917 (1995).
- [23] S. Larochelle, A. Talebpour, and S. L. Chin, *J. Phys. B: At. Mol. Opt. Phys.* **31**, 1201 (1998).
- [24] A. Becker and F. H. M. Faisal, *Phys. Rev. A* **59**, R3182 (1999); *J. Phys. B: At. Mol. Opt. Phys.* **32**, L335 (1999).
- [25] H. Maeda, M. Dammasch, U. Eichmann, W. Sandner, A. Becker, and F. H. M. Faisal, *Phys. Rev. A* **62**, 035402 (2000).
- [26] H. Maeda, M. Dammasch, U. Eichmann, and W. Sandner, *Phys. Rev. A* **63**, 025401 (2001).
- [27] S. Palaniyappan *et al.*, *J. Phys. B: At. Mol. Opt. Phys.* **39**, S357 (2006).
- [28] K. I. Dimitriou, S. Yoshida, J. Burgdörfer, H. Shimada, H. Oyama, and Y. Yamazaki, *Phys. Rev. A* **75**, 013418 (2007).
- [29] S. Yoshida, K. I. Dimitriou, J. Burgdörfer, H. Shimada, H. Oyama, and Y. Yamazaki, *J. Phys.: Conf. Ser.* **163**, 012009 (2009).
- [30] J. S. Cohen, *Phys. Rev. A* **64**, 043412 (2001).
- [31] K. I. Dimitriou, D. G. Arbo, S. Yoshida, E. Persson, and J. Burgdörfer, *Phys. Rev. A* **70**, 061401(R) (2004).
- [32] D. B. Milošević, G. G. Paulus, D. Bauer, and W. Becker, *J. Phys. B: At. Mol. Opt. Phys.* **39**, R203 (2006).
- [33] N. Hazewindus and J. M. Van Nieuwland, United States Patent 4019989 (1977).
- [34] L. D. Landau and E. M. Lifshitz, *Quantum Mechanics Non-Relativistic Theory*, 2nd ed. (Pergamon, Oxford, 1965), Sec. 77.
- [35] A. M. Perelomov, V. S. Popov, and M. V. Terent'ev, *Zh. Eksp. Teor. Fiz.* **51**, 309 (1966) [Sov. Phys. JETP **24**, 207 (1966)].
- [36] M. V. Ammosov, N. B. Delone, and V. P. Krainov, *Zh. Eksp. Teor. Fiz.* **91**, 2008 (1986) [Sov. Phys. JETP **64**, 1191 (1987)].
- [37] V. S. Popov, *Usp. Fiz. Nauk* **174**, 921 (2004) [*Phys. Usp.* **47**, 855 (2004)].
- [38] V. P. Krainov and B. Shokri, *Zh. Eksp. Teor. Fiz.* **107**, 1180 (1995) [JETP **80**, 657 (1995)].
- [39] V. P. Krainov, *J. Opt. Soc. Am. B* **14**, 425 (1997).
- [40] D. Bauer and P. Mulser, *Phys. Rev. A* **59**, 569 (1999).
- [41] V. S. Popov, *Zh. Eksp. Teor. Fiz.* **118**, 56 (2000) [Sov. Phys. JETP **91**, 48 (2000)].
- [42] X. M. Tong and C. D. Lin, *J. Phys. B: At. Mol. Opt. Phys.* **38**, 2593 (2005).
- [43] R. J. Damburg and V. V. Kolosov, *J. Phys. B: At. Mol. Opt. Phys.* **9**, 3149 (1976); **11**, 1921 (1978).
- [44] V. Franceschini, V. Grecchi, and H. J. Silverstone, *Phys. Rev. A* **32**, 1338 (1985).
- [45] V. M. Vainberg, V. D. Mur, V. S. Popov, and A. V. Sergeev, *Pis'ma Zh. Eksp. Teor. Fiz.* **44**, 9 (1986) [Sov. Phys. JETP Lett. **44**, 9 (1986)]; *Zh. Eksp. Teor. Fiz.* **93**, 450 (1987) [Sov. Phys. JETP **66**, 258 (1987)].
- [46] V. S. Popov *et al.*, *Phys. Lett. A* **124**, 77 (1987); *ibid.* **149**, 418 (1990); V. D. Mur and V. S. Popov, *Laser Phys.* **3**, 462 (1993).
- [47] W. H. Press, S. A. Teukolsky, W. T. Vetterling, and B. P. Flannery, *Numerical Recipes in Fortran 77: The Art of Scientific Computing*, 2nd ed. (Cambridge University, Cambridge, 1992).
- [48] C. W. Gear, *Numerical Initial Value Problems in Ordinary Differential Equations* (Prentice-Hall, Englewood Cliffs, NJ, 1971).
- [49] G. Sansone, C. Vozzi, S. Stagira, M. Pascolini, L. Poletto, P. Villoresi, G. Tondello, S. De Silvestri, and M. Nisoli, *Phys. Rev. Lett.* **92**, 113904 (2004).